Nanoscale

ROYAL SOCIETY OF CHEMISTRY

PAPER

View Article Online
View Journal | View Issue

Cite this: *Nanoscale*, 2020, **12**, 16359

A metal–organic framework based inner ear delivery system for the treatment of noise-induced hearing loss†

Xiaoxiang Xu,*‡[a] Kun Lin,‡[b] Yanzhi Wang,‡[c] Kai Xu,[b] Yu Sun,[b] Xiuping Yang,[a] Minlan Yang,[a] Zuhong He,[b] Ya Zhang,[a] Haoquan Zheng *[c] and Xiong Chen*[a]

Received 28th June 2020,
Accepted 15th July 2020

DOI: 10.1039/d0nr04860g

rsc.li/nanoscale

Noise-induced hearing loss (NIHL) is associated with both acute and chronic noise exposure. The application of steroid hormones is the first-line treatment for NIHL. However, a high dose of steroid hormone in the body is necessary to maintain its efficacy and causes side effects, such as headache and osteoporosis. In this work, we prepared a zeolitic imidazolate framework (ZIF)-based system for steroid hormone delivery in the inner ear. Methylprednisolone (MP), a typical steroid hormone, was encapsulated into ZIF-90 nanoparticles (NPs) using one-pot synthesis method. The obtained MP@ZIF-90 NPs are negatively charged and 120 nm in size and showed good biocompatibility and stability at a pH value of 7.4. After intraperitoneal injection, ZIF-90 could efficiently protect drugs during peripheral blood circulation, enter the inner ear *via* the blood labyrinthine barrier (BLB) and slowly release the drugs. Auditory brainstem response (ABR) tests indicated that MP@ZIF-90 exhibits better protection of mice from noise than those using the free MP and ZIF-8 with encapsulated MP (MP@ZIF-8). More importantly, MP@ZIF-90 showed no defects to the inner ear after being treated for noise and low nephrotoxicity during therapy, which demonstrates the biocompatibility of this material. We believe the ZIF-90 based delivery system is an efficient strategy for inner ear therapy of NIHL.

Introduction

Hearing loss (HL) is a common sensory disability all over the world.[1–3] Both acute and chronic noise exposure causes noise-induced hearing loss (NIHL) by the formation of free radicals, which overwhelm the natural antioxidant system.[4] Scientists have used antioxidants, growth factors, and steroids to protect the ear from damage. In the treatment of NIHL, the application of steroids is the first-line treatment. The steroids are injected into the middle ear to protect the ear and aid hearing.[5–7] However, steroid hormones are discharged rapidly and lose their activity in the middle ear after direct injection.

Various delivery systems, such as intratympanic and hydrogel delivery systems, have been developed and can be considered, potential delivery systems to deliver steroid hormones into the inner ear.[8–11] However, there are some drawbacks associated in using these systems, such as the multi-injection, plating of hydrogel and high dose of agents in the local area of ears, which may cause pain and ototoxicity to patients. Recently, nanoparticle (NP) based delivery systems have been developed for inner ear drug delivery.[12–16] These NP based delivery systems must fulfil several demands: (1) the drug loaded NPs after injection have to enter the inner ear through the blood labyrinthine barrier (BLB), which prevents the entry of NPs into the inner ear;[17] (2) the side effects should be low. These NPs should not cause any defects in the inner ear and have low toxicity in organs.[18,19] However, a NP based delivery system, which not only effectively delivers steroid hormone into the inner ear but also shows low side effects has rarely been reported.

As a subclass of metal–organic frameworks (MOFs), zeolitic imidazole frameworks (ZIFs) are synthesized using Zn/Co ion and imidazole linkers.[20–27] ZIF NPs show great potential as delivery systems for guest molecules, drugs, proteins and RNA

[a]*Department of Otorhinolaryngology-Head and Neck Surgery, Zhongnan Hospital of Wuhan University, Wuhan, 430071, China. E-mail: zn003504@whu.edu.cn, zn_chenxiong@126.com*

[b]*Department of Otolaryngology, Union Hospital, Tongji Medical College, Huazhong University of Science and Technology, Wuhan 430022, China*

[c]*Key Laboratory of Applied Surface and Colloid Chemistry, Ministry of Education, School of Chemistry and Chemical Engineering, Shaanxi Normal University, Xi'an 710119, China. E-mail: zhenghaoquan@snnu.edu.cn*

†Electronic supplementary information (ESI) available: Methods and experimental procedures, structure model of ZIF-90 and MP, SEM images and PXRD patterns and N_2 adsorption/desorption of ZIF-8 and MP@ZIF-8. See DOI: 10.1039/D0NR04860G

‡These authors contributed equally to this work.

due to their high stability and good biocompatibility.[28–38] Recently, ZIF NPs are found to be stable at physiological pH (pH 7.4) *in vitro* for more than 15 days and show good biocompatibility against three cell lines.[29,34,39] In an *in vivo* test, mice that were intravenously administrated with 100 mg kg^{-1} of ZIF-90 NPs could still survive.[40–42] Furthermore, ZIF based NPs show good cellular uptake properties and good enrichment in tumour tissues. After being taken up by cancer cells, the drugs in ZIF NPs were slowly released due to the decomposition of the ZIF framework in the acidic environment in the cancer cells.[28] Therefore, we propose that ZIF NPs represent a promising delivery system for inner ear therapy.

Here, we report a ZIF-based methylprednisolone (MP) delivery system. This newly developed ZIF-based delivery system is used for inner ear therapy for the first time. MP is a commonly used steroid hormone that is used as a model drug for inner ear therapy. ZIF-90 NPs using $Zn(CH_3COO)_2$ as a metal source and imidazolate-2-carboxyaldehyde (2-ICA) as a linker were prepared to immobilize MP and other molecules (Fig. 1). The location and distribution of the ZIF NPs in the inner ear of mice were investigated by *in vitro* imaging. The auditory function of the injected mice was tested to show the protective effect under noise models. Cochlear tissue confocal imaging and blood biochemical tests were used to detect potential side effects, including structural defects in the inner ear and toxicity to the organs of the mice. This ZIF-based delivery system combines the characteristics of ZIF itself and its nanoscale advantages. The easy functionalization properties of ZIF, such as the tunability of the functional group on the surface and ability to load molecules and nanoparticles with different functions, will pave the way for the development of designable drug delivery systems for inner ear therapies in the future.

Experimental section

Chemical

$Zn(NO_3)_2{\cdot}6H_2O$ (98%), $Zn(CH_3COO)_2{\cdot}2H_2O$ (98%), and 2-ICA (99%), were purchased from the Energy Chemical, China.

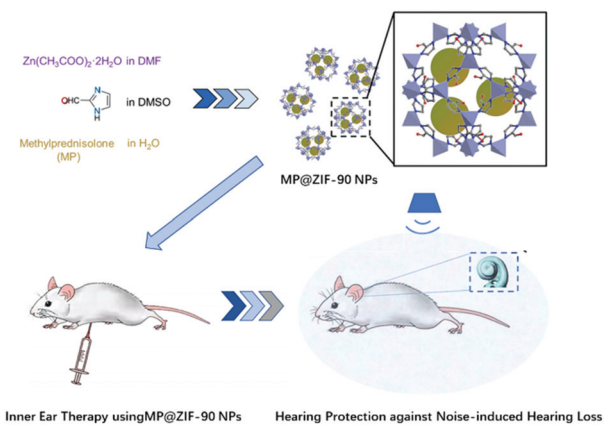

Fig. 1 Schematic illustration of the preparation of MP@ZIF-90 for inner ear therapy.

Methanol (AR, 99.5%), ethanol (AR, 99.7%), *N*,*N*-dimethylformamide (DMF) (AR, 99.5%), Fluorescein isothiocyanate (FITC), and Dimethyl sulfoxide (DMSO) (AR, 99.5%) were purchased from the Tianjin Fuyu Fine Chemical, China. MP sodium succinate for injection was purchased from the Pfizer, USA. All the reagents were of analytical grade and used as received without further purification. Deionized water was used throughout the experimental processes. All of the C57BL/6J mice were purchased from, raised and fed in the specific-pathogen-free Experimental Animal Centre of Huazhong University of Science and Technology. All efforts were made to minimize animal suffering and to reduce the number of animals used. All animal procedures were performed in accordance with the Guidelines for Care and Use of Laboratory Animals of Animal Research of Tongji Medical College, Huazhong University of Science and Technology and approved by the Animal Ethics Committee of Tongji Medical College, Huazhong University of Science and Technology.

Synthesis of MP@ZIF-90

20 mg of MP was dissolved in 400 μL of deionized water. 2 mmol of 2-ICA was dissolved in 20 mL of DMSO. The MP solution and 2-ICA solution were mixed under stirring. After 5 min, 10 mL of $Zn(CH_3COO)_2{\cdot}2H_2O$ (0.2 M) in DMF was added into and stirred at room temperature for 30 min. The mixture was washed by ethanol and dried in the freeze dryer for 24 h. Then, the powders were re-dispersed in PBS solution/ethanol and treated with ultrasound for 30 min for further bioapplications.

To measure the loading of MP, 10 mg of MP@ZIF-90 was dissolved in 0.1 M HCl. The above solution was dispersed in a mixed solution (the CH_3OH : 0.01 M KH_2PO_4 (v/v %) ratio was 65 : 35). The loading of MP in MP@ZIF-90 was determined by RP-HPLC from the absorbance at 254 nm. The loading amount in MP@ZIF-90 was calculated by the equation: MP loading% = $m_{MP}/m_{MP@ZIF\text{-}90}$.

In vitro imaging of ZIF-90 based NPs in the inner ear of mice

C57BL/6J mice, 4–5 weeks old, were used. The mice were randomly assigned to nine groups (n = 3): Group 1, group 2, and group 3 were treated with PBS solutions (denoted as control), FITC@ZIF-90 and FITC@ZIF-8, respectively, and they were evaluated on the 1st day after administration; group 4, group 5, and group 6 were evaluated on the 3rd day after administration; group 7, group 8, and group 9 were evaluated on the 9th day after administration. The concentrations of FITC@ZIF-90 and FITC@ZIF-8 were 7.5 mg mL^{-1} in PBS solution. The above suspensions were sonicated for 120 minutes and then were administered to mice with a dose of 150 mg kg^{-1} mice weight by intraperitoneal injection. After injection on the designated days, the mice were anesthetized completely by a mixed anaesthesia solution of ketamine and chlorpromazine. Then, the inner ear tissues of the mice were taken out quickly and monitored by an *in vivo* imaging device (Lago X, SI Imaging). The samples were examined at excitation/emission wavelengths of 490/535 nm.

Examination of auditory function (auditory brainstem response, ABR) before and after noise intervention

A total of 24 C57BL/6J mice, 4–5 weeks old, were divided into four groups: the free MP group (n = 6), MP@ZIF-90 group (n = 6), MP@ZIF-8 group (n = 6) and control group (n = 6). In the free MP group, the solvent was a phosphate-buffered saline (PBS) solution (pH 7.4) with 3.3 mg mL^{-1} MP. Then, the above solution was administered to mice at a dose of 60 mg kg^{-1} by intraperitoneal injection. In the MP@ZIF-90 and MP@ZIF-8 groups, the MP@ZIF-90/MP@ZIF-8 NPs were suspended into a PBS solution. The final concentration of MP in the suspension was 10 mg mL^{-1}. In order to get a homogenous suspension, the suspensions were sonicated for 20 min in an ultrasonic crusher and then were administered to mice with a dose of 180 mg kg^{-1} by intraperitoneal injection. In the control group, only PBS solutions were used, which was also administered to the mice by intraperitoneal injection. The injection volume of the PBS solution was based on the volume of the solution given in the corresponding experimental groups.

Then, the mice were subjected to white noise. White noise at 100 dB SPL was applied to the mice for 3 h per day for 3 consecutive days. Loudspeakers with a determined intensity were placed about 15 cm above the animal feeding cage. The difference in noise intensity within the range of animal activity was not more than ±2 dB. The interference noise was calibrated and measured with a tes-1351b sound level meter before being put into the range. The animals were placed in a feeding cage about 45 × 45 × 20 cm^3 below the loudspeaker.

ABR detections were carried out before and after the injections for comparison. The mice were fully anesthetized by intraperitoneal injection with a mixture of ketamine (120 mg kg^{-1}) and chlorpromazine (20 mg kg^{-1}) and then were transferred to a heating pad in the sound insulation room. Three electrodes were placed under the skin of the mice. The recording electrode were located at the vertex, the reference electrode were in the tested ear, and the ground electrode was at the contralateral ear. Short pure tones of 8, 16, 24, and 32 kHz were used as stimulus sounds. The speaker was placed about 5 cm near the external auditory canal of the audiometry ear. The ABR observation window was 10 ms and the signal was overlapped 1024 times. The intensity of the acoustic stimulation started from 90 dB and decreased gradually to 10 dB. When approaching the threshold, it was decreased gradually to 5 dB. The threshold value was determined by the stable and repeatable ABR waveform obtained from the minimum stimulus sound. The accuracy of the instrument was calibrated with a microphone before each test to ensure that the conditions for the ABR detections were the same.

Cochlear tissue preparation and confocal imaging

The mice were deeply anaesthetized and sacrificed and then were quickly decapitated. The cochlea of the mice were removed from the temporal bone. The round and oval windows were opened. The apex of the cochlea was put under the microscope. The cochlea was fixed in 4% paraformaldehyde at 4 °C overnight. After fixation, the cochlea was rinsed with PBS solutions 3 times (10 min each) and was decalcified in 10% EDTA solution for 3 days. The cochlear axis was exposed by removing the volute. We then carefully separated the cochlear basement membrane and divided the basement membrane into apical, middle and basal turns according to the rotation. The separated basement membrane was permeabilized with 0.3% Triton X-100 in PBS solution for 30 min. Finally, 4′,6-diamidine-2′-phenylindole dihydrochloride (DAPI) and phalloidin (0.05 mg mL^{-1}, P5282) were used for nuclear and F-actin staining, respectively. Images were captured with a Leica scanning laser confocal microscope (model LCS SP8 STED, Leica, Wetzlar, Germany).

Blood biochemical test

After being anaesthetized and before extraction of the cochlear, the blood of each mouse was collected by eyeball extraction, with about 500 μL of blood was taken. Then, 150–200 μL of serum was extracted for the renal function test. Then, an Eppendorf (EP) tube containing the blood of the mice was placed at 4 °C. After 1 h, the EP tube was placed in a low-temperature high-speed centrifuge at 4000 rpm for 10 min to extract about 200 μL of supernatant. The extracted supernatant was analyzed with a full-automatic biochemical analyzer (Chemray 240, rayto, China) to detect the renal function, including the concentrations of the serum creatinine (CREA), urea (UREA) and uric acid (UA) of mice.

Results and discussion

ZIF-90, which has been used for delivery systems for various drugs and biomolecules, was self-assembled from Zn ions and 2-ICA.[42] In a typical synthesis, MP, 2-ICA and $Zn(CH_3COO)_2$ were dissolved in deionized water, DMSO and DMF, respectively. The solutions of MP and 2-ICA were mixed under vigorous stirring. Then, a solution of $Zn(CH_3COO)_2{\cdot}2H_2O$ was added and stirred at room temperature for 30 min. Finally, ZIF-90 NPs with MP encapsulated (MP@ZIF-90) were prepared. The loading percent of MP into MP@ZIF-90 was determined to be 20 wt% based on the equation described in the Experimental section. As shown in Fig. S1,† the molecular diameter of MP is larger than the size of the ZIF-90 structure (3.4 Å), so the immobilized MP molecules are mainly located in the ZIF-90 cage and cannot diffuse out through the pore channel. This is important for the safe protection of MP throughout the blood circulation.

As shown in scanning electron microscopy (SEM) images, the obtained MP@ZIF-90 NPs are sphere-like NPs with a size of around 120 nm (Fig. 2a). The particle size of MP@ZIF-90 is slightly larger than that of pure ZIF-90 (90 nm). The powder X-ray diffraction (PXRD) pattern of MP@ZIF-90 shows sharp diffraction peaks at 2 theta = 7.4°, 14.7° and 29.6°, which were assigned to the (110), (200) and (211) planes of a *sod* type structure, respectively (Fig. 2b). The experimental PXRD result

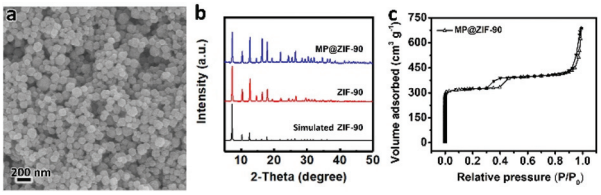

Fig. 2 SEM image (a), PXRD patterns (b) and N_2 adsorption/desorption isotherm (c) of MP@ZIF-90.

fits well with the simulated PXRD pattern and that from previous report, indicating the successful preparation of highly crystalline ZIF-90.[40] Furthermore, no diffraction peak assigned to free MP was observed in the PXRD pattern, indicating the MP molecules were homogenously distributed inside the ZIF-90 materials. The N_2 adsorption/desorption isotherm of MP@ZIF-90 shows a sharp capillary condensation at low pressure ($<P/P_0$ = 0.1), indicating that MP@ZIF-90 possesses abundant micropores in its ordered porous framework. The Brunauer–Emmett–Teller (BET) surface areas and total pore volume of MP@ZIF-90 are 1029 $m^2\ g^{-1}$ and 1.05 $cm^3\ g^{-1}$ (Fig. 2c), respectively. We further measured the particle size of MP@ZIF-90 by dynamic light scattering (DLS) in 0.1 M PBS (pH 7.4). The average particle size of MP@ZIF-90 was 105 nm with a polydispersity index (PDI) of 0.22 (Fig. 3a). As previously reported, NPs with a particle size of 50–200 nm are the most efficient for bio-related applications. The loading of MP in MP@ZIF-90 occurred at 20 wt%, which was calculated based on the equation in Experimental section. When the loading was further increased, the particle size of MP@ZIF-90 was broadened, which weakens its ability as a drug delivery system. We further investigated the stability of MP@ZIF-90 at a physiological pH (7.4) and the location of MP in MP@ZIF-90 by obtaining an *in vitro* release profile of MP (Fig. 3b). MP@ZIF-90 shows no release at pH 7.4 for 7 days, indicating the MP molecules are encapsulated in the framework of MP@ZIF-90. Moreover, ZIF-90 was found to be sensitive to acid or ATP. When the pH was adjusted to 5, MP was slowly released within 36 h due to the decomposition of ZIF-90, which is a similar result to that found in a previous report.[30,33] Therefore, MP loaded ZIF-90 materials were successfully prepared in one pot and could safely protect MP under physiological conditions.

ZIF-8 NP is another typical MOF that is widely used as a delivery system for drugs, enzymes, proteins and DNA. ZIF-8 has the same topological structure as ZIF-90 but uses different types of imidazole linkers. MP@ZIF-8 was prepared for comparison (Fig. S2 and S3†). The zeta potentials of ZIF-90, MP@ZIF-90, ZIF-8 and MP@ZIF-8 were obtained using a Zeta analyzer (DelsaNano C, Beckman Coulter, Inc.) and are −5.1, −6.9, +25.3, and +19.3 mV in 0.1 M PBS (pH 7.4) at room temperature, respectively (Fig. 3c). The N in the 2-methylimidazolate in ZIF-8 is easily protonated, which makes ZIF-8 positively charged, while the carboxyaldehyde group in ZIF-90 is negatively charged in 0.1 M PBS (pH 7.4). We further evaluated the *in vitro* biocompatibility of the MP@ZIF-90 and MP@ZIF-8 in MCF-7 cells by MTT assays (Fig. 3d). The cell viability with MP@ZIF-90 is higher than that using MP@ZIF-8, which indicates that MP@ZIF-90 is more biocompatible. Positively charged ZIF-8 NPs are beneficial for anti-cancer therapy due to their good cellular uptake properties, which is caused by the strong interaction between the positively charged ZIF-8 NPs and negatively charged cell membrane. However, in inner ear therapy, this cellular uptake property might induce the formation of defects in inner hair cells (IHC) and outer hair cells (OHC). Therefore, slightly negatively charged MP@ZIF-90 NP show a good biocompatibility and has potential to be used in inner ear therapy for NIHL.

We further used the ZIF NPs for inner ear therapy. The distribution of the ZIF NPs in the inner ear after intraperitoneal injection was first investigated. The MP molecules show no fluorescence signal. Thus, FITC@ZIFs were selected as a model to investigate the location of the ZIF NPs in the inner ear of the mice (Fig. S4 and S5†). The same imaging settings were used for all of the images. As shown in Fig. 4, none of the images in the control group showed a fluorescence signal, indicating that the mice fed for different times caused no large difference. After intraperitoneal injection of FITC@ZIF-90 for 1 day, the image of the cochlea of the mice showed a strong fluorescence signal assigned to FITC, which implies that FITC@ZIF-90 can enter the inner ear of the mice through blood circulation. After 3 days of administration, the intensity slightly decreased, while the FITC signal from FITC@ZIF-90 was still observed after 9 days of administration. Therefore, the FITC@ZIF-90 could enter the inner ear and slowly release the FITC for up to 9 days. For the FITC@ZIF-8 system, similar results were observed. Our results indicate that the ZIF-90 and ZIF-8 NPs could enter the inner ear through the BLB and

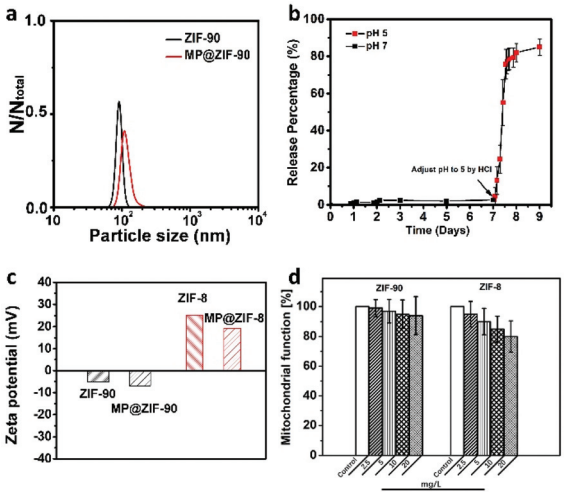

Fig. 3 (a) DLS data of ZIF-90 and MP@ZIF-90. (b) Release profile of MP@ZIF-90 at pH 7.4 and changed to 5 after 7 days. (c) Zeta potential of ZIF-90, MP@ZIF-90, ZIF-8 and MP@ZIF-8. (d) Function of mitochondria of ZIF-90 and ZIF-8 in MCF-7 cells treated for 48 h. Results are presented as means ± standard deviation (s.d.) (n = 3).

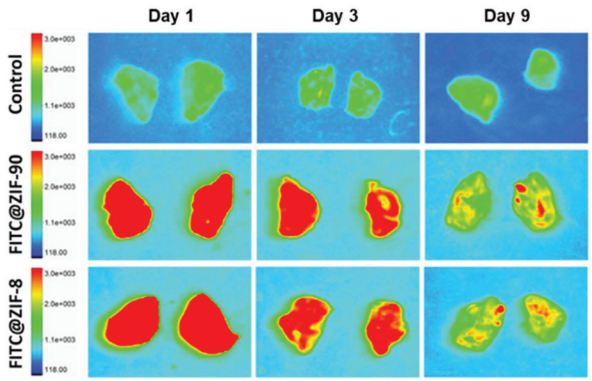

Fig. 4 *In vitro* imaging of the cochlear of C57BL/6J mice after the administration of FITC@ZIF-8&FITC@ZIF-90 at 1, 3, and 9 days.

release the active drugs at a suitable concentration during inner ear therapy.

In order to investigate the NIHL of the mice before and after inner ear therapy, auditory brainstem response (ABR) tests were carried out using a Tucker-Davis Technologies System (RZ6, Tucker Davis Tech. Inc., Alachua, FL, USA) (Fig. 5a). The low ABR threshold of the mice indicates a good protection. As shown in Fig. 5b, the results of the ABR tests on the mice before injection showed that none of the hearing thresholds of the mice in any of the groups exhibited a significant difference at a click of 8–32 kHz ($P > 0.05$), indicating that the mice in the selected groups were suitable for further hearing investigations. The mice in the control group were exposed to 100 dB SPL of white noise for three consecutive days with a three-hour treatment per day. The mice that were not given the drug showed the most significant impact at high frequency, 16–32 kHz. The mean values of hearing loss at 16, 24, and 32 kHz were more than 25 dB, while the hearing loss at 16 kHz was the most serious (36.7 ± 5.2 dB). The ABR detection results at the low frequency of 8 kHz in the hearing threshold also showed a significant hearing loss ($P < 0.05$). Therefore, the mice that were not given the drug have an obvious hearing loss under induced noise, indicating that the inner ear therapy is necessary.

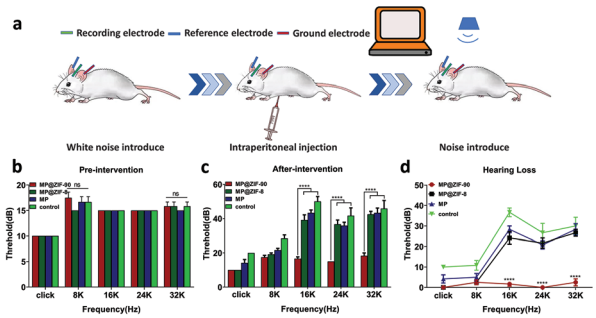

Fig. 5 (a) Scheme of ABR test results of the mouse models. The ABR test results of the mice before noise intervention (b), after noise intervention (c) and the mice's hearing loss (d). Results are presented as means ± standard deviation (s.d.) ($n = 6$).

The ABR tests of the mice using free MP, MP@ZIF-90, and MP@ZIF-8 are shown in Fig. 5b–d. The hearing of the mice in the free MP group still shows a significant loss and no protective effects compared to the mice in the control group ($P > 0.05$) at 8–32 kHz. Notably, the mice in the MP@ZIF-90 group exhibit obvious protective effects even after being treated with high frequency noise (16 kHz, 24 kHz, and 32 kHz). At these high frequencies, the difference in the ABR thresholds between the MP@ZIF-90 group and the other three groups (control, free MP, and MP@ZIF-8) is very significant ($P < 0.0001$). The mice in the MP@ZIF-90 group exhibit no hearing loss at click and 24 kHz. As shown in Fig. 5d, the ABR thresholds of the mice treated with MP@ZIF-90 at 8 kHz, 16 kHz and 32 kHz were only 5 dB higher than those of the mice without any noise treatment (Fig. 5d). On the other hand, in the MP@ZIF-8 group, the ABR thresholds of the mice treated with MP@ZIF-8 were 10 dB, 8.33 dB, and 12.5 dB, which are lower than the levels in the control groups at click, 8 kHz, and 16 kHz, respectively (Fig. 5c). However, at high frequency (24 kHz and 32 kHz), there was no significant difference between the mice in the MP@ZIF-8 and control groups (both $P = 1.00 > 0.06$). All the results above indicate that MP@ZIF-90 is highly efficient for hearing protection from induced noise and performs better than free MP and MP@ZIF-8. Therefore, MP@ZIF-90 is an efficient delivery system for inner ear therapy because it offers good protection of the mice from noise.

To further demonstrate the safe use of the ZIF-based NP delivery system for inner ear therapy, confocal images of the inner ear and blood biochemical tests after the inner ear therapy were carried out (Fig. 6 and 7). The confocal images of the basement membrane of the cochlea of the four mouse model groups, which contains inner hair cells (IHC) and outer hair cells (OHC), are shown in Fig. 6. All of the mice in these four groups were treated with noise. The operating procedures were the same as those of the ABR tests. The confocal images show that there were almost no defects in the OHC of the base-

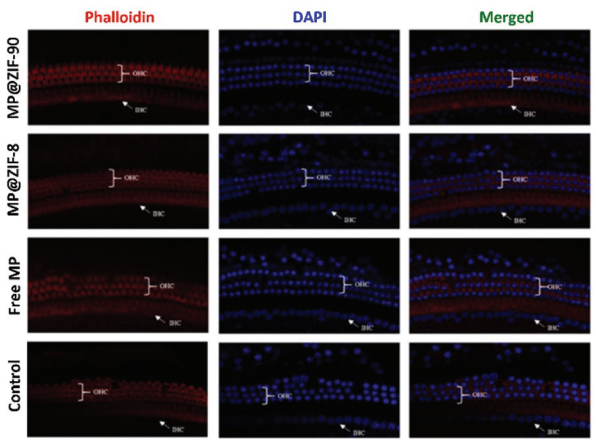

Fig. 6 Confocal images of the basement membrane of the cochlea (including IHC and OHC) for the four mouse model groups. All mice in these four groups were treated with noise. The operating procedures are the same as for the ABR tests.

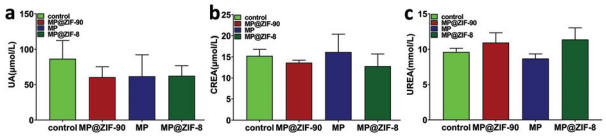

Fig. 7 Renal function test results of UA (a), CREA (b) and UREA (c) in four different mice models, which are denoted as control, MP@ZIF-90, MP and MP@ZIF-8. Results are presented as means ± standard deviation (s.d.) (n = 6).

ment membrane of the cochlea, including the basal, middle and apical turns, indicating a good biocompatibility during inner ear therapy using MP@ZIF-90. For comparison, when control, MP@ZIF-8, and free MP were used, the hair cells on the basement membrane of the cochlea were mainly scattered or absent in the basal turn and middle turn. The hair cells of the apical turn were almost intact. Furthermore, MP@ZIF-90 contains a small amount of negative charges, indicating MP@ZIF-90 could prevent damage to the inner ear structure from noise treatments. Therefore, MP@ZIF-90 could protect the structure of the inner ear from the damage caused by noise.

We further investigated the nephrotoxicity of mice treated with the ZIF-based NPs. Renal function test results of serum creatinine (CREA), urea (UREA) and uric acid (UA) were detected by collecting the serum of mice (Fig. 7). The CREA results of mice treated with NP and those treated with free MP groups, MP@ZIF-90, and MP@ZIF-8 showed no significant differences (Fig. 7a). The P values of the control *vs.* free MP, MP@ZIF-90, and MP@ZIF-8 were 1.000, 1.000, and 0.256, respectively, all >0.05. There were also no significant toxicities observed in the renal functions of UREA and UA for the free MP, MP@ZIF-90, and MP@ZIF-8 groups relative to the control group (Fig. 7b and c). All of these results indicate that the MP-loaded ZIF based systems are potential delivery systems for inner ear therapy due to their low nephrotoxicity, low side effects and good biocompatibility.

Conclusions

We have prepared a ZIF-based NP system for steroid hormone delivery, which was used for inner ear therapy for the first time. MP@ZIF-90 possesses a homogenous particle size of around 120 nm, a highly ordered crystalline structure, and good biocompatibility. The nano-sized particles could enter the inner ear through the BLB, while ZIF-90 could slowly release MP at a determined concentration. The slightly negative charge of MP@ZIF-90 prevented side effects from occurring in the inner ear. Following intraperitoneal injection of MP@ZIF-90, *in vitro* imaging results of the cochlea of the mice indicated FITC@ZIF-90 could enter the inner ear through the BLB and slowly release the drugs for up to 9 days. MP@ZIF-90 exhibited much better protection of mice from noise based on ABR tests compared to free MP and MP@ZIF-8. Moreover, MP@ZIF-90 prevented defects in the inner ear following treatment with noise, and low nephrotoxicity was observed during therapy, which demonstrates the biocompatibility and low side effects of this material. Therefore, ZIF-90 is a potential delivery system for a steroid hormone, which is an efficient method for inner ear therapy of NIHL. We believe that the reported results provide insights for novel drug delivery systems for inner ear therapy.

Conflicts of interest

There are no conflicts to declare.

Acknowledgements

We acknowledge the finical support from the National Natural Science Foundation of China (No. 81570903, 21975148 and 21601118), the Fundamental Research Funds for the Central Universities (GK201903033).

Notes and references

1 L. Li, T. Chao, J. Brant, B. O'Malley, A. Tsourkas and D. Li, *Adv. Drug Delivery Rev.*, 2017, **108**, 2–12.
2 A. A. McCall, E. E. L. Swan, J. T. Borenstein, W. F. Sewell, S. G. Kujawa and M. J. McKenna, *Ear Hear.*, 2010, **31**, 156–165.
3 L. P. Rybak, A. Dhukhwa, D. Mukherjea and V. Ramkumar, *Front. Cell. Neurosci.*, 2019, **13**, 300.
4 D. Henderson, E. C. Bielefeld, K. C. Harris and B. H. Hu, *Ear Hear.*, 2006, **27**, 1–19.
5 S.-H. Lee, A.-R. Lyu, S.-A. Shin, S.-H. Jeong, S.-A. Lee, M. J. Park and Y.-H. Park, *Sci. Rep.*, 2019, **9**, 12646.
6 I. Meltser and B. Canlon, *Hear. Res.*, 2011, **281**, 47–55.
7 R. Guo, S. Zhang, M. Xiao, F. Qian, Z. He, D. Li, X. Zhang, H. Li, X. Yang, M. Wang, R. Chai and M. Tang, *Biomaterials*, 2016, **106**, 193–204.
8 S. A. Lajud, Z. Han, F.-L. Chi, R. Gu, D. A. Nagda, O. Bezpalko, S. Sanyal, A. Bur, Z. Han, B. W. O'Malley and D. Li, *J. Controlled Release*, 2013, **166**, 268–276.
9 L. Xu, J. Heldrich, H. Wang, T. Yamashita, S. Miyamoto, A. Li, C. E. Uboh, Y. You, D. Bigelow, M. Ruckenstein, B. O'Malley and D. Li, *Otol. Neurotol.*, 2010, **31**, 1115–1121.
10 P. Xia, E. K. Raulerson, D. Coleman, C. S. Gerke, L. Mangolini, M. L. Tang and S. T. Roberts, *Nat. Chem.*, 2020, **12**, 137–144.
11 W. Li, J. Wu, J. Yang, S. Sun, R. Chai, Z.-Y. Chen and H. Li, *Proc. Natl. Acad. Sci. U. S. A.*, 2015, **112**, 166.
12 M. N. Kayyali, J. R. A. Wooltorton, A. J. Ramsey, M. Lin, T. N. Chao, A. Tsourkas, B. W. O'Malley and D. Li, *J. Controlled Release*, 2018, **279**, 243–250.
13 R. Mittal, S. A. Pena, A. Zhu, N. Eshraghi, A. Fesharaki, E. J. Horesh, J. Mittal and A. A. Eshraghi, *Artif. Cells, Nanomed., Biotechnol.*, 2019, **47**, 1312–1320.

14 H. Meyer, T. Stöver, F. Fouchet, G. Bastiat, P. Saulnier, W. Bäumer, T. Lenarz and V. Scheper, *Int. J. Nanomed.*, 2012, **7**, 2449–2464.
15 Z. He, S. Sun, M. Waqas, X. Zhang, F. Qian, C. Cheng, M. Zhang, S. Zhang, Y. Wang, M. Tang, H. Li and R. Chai, *Sci. Rep.*, 2016, **6**, 29621.
16 H. Li, L.-L. Tan, P. Jia, Q.-L. Li, Y.-L. Sun, J. Zhang, Y.-Q. Ning, J. Yu and Y.-W. Yang, *Chem. Sci.*, 2014, **5**, 2804–2808.
17 S. N. Bowe and A. Jacob, *Curr. Opin. Otolaryngol. Head Neck Surg.*, 2010, **18**, 377–385.
18 G. D. Chen, D. M. Daszynski, D. Ding, H. Jiang, T. Woolman, K. Blessing, P. F. Kador and R. Salvi, *Hear. Res.*, 2020, **388**, 107880.
19 Z. He, L. Guo, Y. Shu, Q. Fang, H. Zhou, Y. Liu, D. Liu, L. Lu, X. Zhang, X. Ding, D. Liu, M. Tang, W. Kong, S. Sha, H. Li, X. Gao and R. Chai, *Autophagy*, 2017, **13**, 1884–1904.
20 A. Phan, C. J. Doonan, F. J. Uribe-Romo, C. B. Knobler, M. O'Keeffe and O. M. Yaghi, *Acc. Chem. Res.*, 2010, **43**, 58–67.
21 H.-C. J. Zhou and S. Kitagawa, *Chem. Soc. Rev.*, 2014, **43**, 5415–5418.
22 T. Islamoglu, S. Goswami, Z. Li, A. J. Howarth, O. K. Farha and J. T. Hupp, *Acc. Chem. Res.*, 2017, **50**, 805–813.
23 K. Sumida, D. L. Rogow, J. A. Mason, T. M. McDonald, E. D. Bloch, Z. R. Herm, T.-H. Bae and J. R. Long, *Chem. Rev.*, 2012, **112**, 724–781.
24 Y. V. Kaneti, S. Dutta, M. S. A. Hossain, M. J. A. Shiddiky, K.-L. Tung, F.-K. Shieh, C.-K. Tsung, K. C. W. Wu and Y. Yamauchi, *Adv. Mater.*, 2017, **29**, 1700213.
25 P.-Q. Liao, W.-X. Zhang, J.-P. Zhang and X.-M. Chen, *Nat. Commun.*, 2015, **6**, 8697.
26 H. Furukawa, K. E. Cordova, M. O'Keeffe and O. M. Yaghi, *Science*, 2013, **341**, 1230444.
27 J. Yang and Y.-W. Yang, *Small*, 2020, **16**, 1906846.
28 J. Zhuang, C.-H. Kuo, L.-Y. Chou, D.-Y. Liu, E. Weerapana and C.-K. Tsung, *ACS Nano*, 2014, **8**, 2812–2819.
29 Q. Wu, M. Niu, X. Chen, L. Tan, C. Fu, X. Ren, J. Ren, L. Li, K. Xu, H. Zhong and X. Meng, *Biomaterials*, 2018, **162**, 132–143.
30 Z. Jiang, Y. Wang, L. Sun, B. Yuan, Y. Tian, L. Xiang, Y. Li, Y. Li, J. Li and A. Wu, *Biomaterials*, 2019, **197**, 41–50.
31 M.-X. Wu and Y.-W. Yang, *Adv. Mater.*, 2017, **29**, 1606134.
32 K. Lu, T. Aung, N. Guo, R. Weichselbaum and W. Lin, *Adv. Mater.*, 2018, **30**, 1707634.
33 J. Deng, K. Wang, M. Wang, P. Yu and L. Mao, *J. Am. Chem. Soc.*, 2017, **139**, 5877–5882.
34 Y. Zhang, F. Wang, C. Liu, Z. Wang, L. Kang, Y. Huang, K. Dong, J. Ren and X. Qu, *ACS Nano*, 2018, **12**, 651–661.
35 F. Lyu, Y. Zhang, R. N. Zare, J. Ge and Z. Liu, *Nano Lett.*, 2014, **14**, 5761–5765.
36 L. Xing, H. Zheng, Y. Cao and S. Che, *Adv. Mater.*, 2012, **24**, 6433–6437.
37 H. Zheng, Y. Zhang, L. Liu, W. Wan, P. Guo, A. M. Nyström and X. Zou, *J. Am. Chem. Soc.*, 2016, **138**, 962–968.
38 J. Yang and Y.-W. Yang, *View*, 2020, **1**, e20.
39 T.-T. Chen, J.-T. Yi, Y.-Y. Zhao and X. Chu, *J. Am. Chem. Soc.*, 2018, **140**, 9912–9920.
40 H. Cheng, X.-Y. Jiang, R.-R. Zheng, S.-J. Zuo, L.-P. Zhao, G.-L. Fan, B.-R. Xie, X.-Y. Yu, S.-Y. Li and X.-Z. Zhang, *Biomaterials*, 2019, **195**, 75–85.
41 T. Baati, L. Njim, F. Neffati, A. Kerkeni, M. Bouttemi, R. Gref, M. F. Najjar, A. Zakhama, P. Couvreur, C. Serre and P. Horcajada, *Chem. Sci.*, 2013, **4**, 1597–1607.
42 W. Morris, C. J. Doonan, H. Furukawa, R. Banerjee and O. M. Yaghi, *J. Am. Chem. Soc.*, 2008, **130**, 12626–12627.